J Biomol NMR (2009) 44:225–233
DOI 10.1007/s10858-009-9332-0

ARTICLE

Histidine side-chain dynamics and protonation monitored by ^{13}C CPMG NMR relaxation dispersion

Mathias A. S. Hass · Ali Yilmaz · Hans E. M. Christensen · Jens J. Led

Received: 6 April 2009 / Accepted: 28 May 2009 / Published online: 17 June 2009

Abstract The use of ^{13}C NMR relaxation dispersion experiments to monitor micro-millisecond fluctuations in the protonation states of histidine residues in proteins is investigated. To illustrate the approach, measurements on three specifically ^{13}C labeled histidine residues in plastocyanin (PCu) from *Anabaena variabilis* (*A.v.*) are presented. Significant Carr-Purcell-Meiboom-Gill (CPMG) relaxation dispersion is observed for $^{13}C^{\varepsilon 1}$ nuclei in the histidine imidazole rings of *A.v.* PCu. The chemical shift changes obtained from the CPMG dispersion data are in good agreement with those obtained from the chemical shift titration experiments, and the CPMG derived exchange rates agree with those obtained previously from ^{15}N backbone relaxation measurements. Compared to measurements of backbone nuclei, $^{13}C^{\varepsilon 1}$ dispersion provides a more direct method to monitor interchanging protonation states or other kinds of conformational changes of histidine side chains or their environment. Advantages and shortcomings of using the $^{13}C^{\varepsilon 1}$ dispersion experiments in combination with chemical shift titration experiments to obtain information on exchange dynamics of the histidine side chains are discussed.

Keywords Plastocyanin · Histidine side-chain dynamics · ^{13}C CPMG NMR relaxation dispersion

Abbreviations

CPMG	Carr-Purcell-Meiboom-Gill
PCu	Plastocyanin

Introduction

Histidine residues are of profound functional importance to many proteins. Among the key properties of histidines are their ability to change the protonation state at physiological pH and to bind metal ions. For example, the interconversion between different protonation states of the imidazole group is required for catalysis of numerous enzymes that rely on general acid/base catalysis (Fersht 1998). Therefore, studies of the kinetics and thermodynamics of these interconversions provide insight into the dynamics and function of histidine-containing active sites. NMR is the most powerful technique to identify the different protonation states of histidine residues, including the fully protonated form and the two tautomers of the imidazole ring (Mandel 1965; Markley 1975; Pelton et al. 1993; Day et al. 2003; Perez-Canadilllas et al. 2003; Shimahara et al. 2007; Grey et al. 2006). Furthermore, NMR relaxation experiments such as Carr-Purcell-Meiboom-Gil (CPMG) relaxation dispersion experiments can be used to characterize the exchange between these different forms (Hass et al. 2008a). Relaxation

M. A. S. Hass · A. Yilmaz · J. J. Led (✉)
Department of Chemistry, University of Copenhagen, Universitetsparken 5, 2100 Copenhagen Ø, Denmark
e-mail: led@kiku.dk

H. E. M. Christensen
Department of Chemistry, The Technical University of Denmark, Kemitorvet 207, 2800 Lyngby, Denmark

Present Address:
M. A. S. Hass
Institute of Chemistry, Leiden University, Einsteinweg 55, 2333 Leiden, The Netherlands

Present Address:
A. Yilmaz
Department of Medicinal Chemistry, Faculty of Pharmaceutical Sciences, University of Copenhagen, Universitetsparken 2, 2100 Copenhagen Ø, Denmark

dispersion techniques, in particular, are well suited to extract quantitative information about exchange processes on the micro-to-millisecond time scale (Palmer et al. 2001). In principle, this information is also encoded in the shape of the NMR signals (Sudmeier et al. 1980). However, the line shapes of the protein NMR signals usually only provide qualitative information about exchange processes.

Histidine dynamics has been characterized using the resonances of nearby ^{15}N backbone nuclei (Hass et al. 2004; Kovrigin and Loria 2006; Grey et al. 2006). However, monitoring the histidine dynamics through nuclei within the imidazole group itself, such as the imidazole ^{13}C nuclei may offers several advantages compared to ^{15}N backbone measurements, in particular in combination with specific ^{13}C labeling of the imidazole ring. Thus, besides providing (1) direct reporters on histidine side-chain dynamics, (2) the imidazole ^{13}C approach, unlike the backbone ^{15}N based methods, only requires assignment of ^{1}H–^{13}C HSQC spectrum of the ^{13}C labeled histidine residues, as the relatively few signals in the spectrum will reduce complications arising from signal overlap. Furthermore, (3) the shorter ^{13}C pulse length compared to the ^{15}N pulse length allows faster CPMG pulsing and thereby faster exchange processes to be studied by ^{13}C CPMG dispersion.

In principle, all ^{13}C, ^{15}N, and non-exchangeable ^{1}H nuclei of the imidazole group could be used to monitor the interchange of protonation states. The $H^{\varepsilon 1}$ and $H^{\delta 2}$ are usually detectable and have been utilized to study histidine protonation using line-shape analysis (Sudmeier et al. 1980). Also ^{1}H relaxation dispersion experiments have been developed but remain less accurate, mainly because strong dipole-dipole couplings to other protons complicate the ^{1}H relaxation dispersion experiments (Ishima and Torchia 2003). For ^{13}C and ^{15}N nuclei such complications are usually negligible. However, the ^{15}N imidazole signals can be line-broadened beyond detection by exchange between protonation states (Pelton et al. 1993). In contrast, the ^{13}C signals of imidazole are less affected by line broadening arising from such processes and are therefore more likely to be detectable than the ^{15}N signals (Sudmeier et al. 1980, 2003). Among the imidazole ^{13}C nuclei, $^{13}C^{\varepsilon 1}$ is the most straightforward nuclei to monitor because the $^{13}C^{\varepsilon 1}$–$H^{\varepsilon 1}$ spin system in the imidazole ring is well approximated by an isolated two-spin system analogous to the ^{15}N–H spin systems in the protein backbone. Therefore, pulse schemes normally used for the backbone ^{15}N CPMG experiments (Loria et al. 1999a; Tollinger et al. 2001) can be used also for the CPMG experiments on the $^{13}C^{\varepsilon 1}$–$H^{\varepsilon 1}$ spin system, as shown recently by (Kovrigin and Loria 2006).

Here we investigate the use of $^{13}C^{\varepsilon 1}$ CPMG dispersion measurements to monitor micro-millisecond fluctuations in the protonation states of histidine residues in proteins. Rates of histidine protonation-deprotonation reported in the literature are on the order of several to many thousands per second (Eigen 1963; Sudmeier et al. 1980; Hass et al. 2007, 2008a). Therefore, exchange between different protonation states is likely to be in the fast exchange regime. This, however, makes a determination of the involved exchange processes difficult since the resonances of a given nucleus in the different exchanging conformations merge into a single average signal. Therefore, when the interconversions are in the fast-exchange regime on the NMR time scale ($k_{ex} > \Delta\omega$), a simultaneous determination of the chemical shifts and the populations of various states from spin relaxation data alone is not possible, even in the simple two-site case, and independent information must be obtained, e.g., from chemical shift titrations in the case of exchange between protonated and deprotonated histidines (Hass et al. 2004).

Here reduced plastocyanin (PCu) from *Anabaena variabilis* (*A.v.*) (Guss et al. 1986; Badsberg et al. 1996; Schmidt et al. 2006) specifically ^{13}C labeled in the histidine imidazole side chains was used as a model system to evaluate the use of $^{13}C^{\varepsilon 1}$ CPMG dispersion measurements. *A.v.* PCu contains three histidines with different binding and protonation characteristics. Two of the histidines, His92 and His39 are involved in Cu(I) binding (Fig. 1). One of the metal binding imidazoles (His92) is exposed to the surface and protonates at acidic pH, whereas the other (His39) is buried inside the protein and does not protonate. The third histidine (His61) is surface exposed and can be protonated or exist in two deprotonated tautomer forms but is not involved in metal binding. The interchange of protonation states of the two histidines His61 and His92 has been studied in detail using various backbone ^{15}N relaxation methods (Hass et al. 2004, 2007, 2008a) and it was found that the protonation of His92 is a two-site exchange process (Hass et al. 2004, 2007), while the protonation of His61 is a more complex three-site exchange process involving both protonation and tautomerization (Hass et al. 2004; 2008a). Here we investigate to what extend information about these exchange processes can be obtained also from CPMG measurements on the $^{13}C^{\varepsilon 1}$ nuclei of the three histidines in *A.v.* PCu.

Materials and methods

Expression and purification of uniformly ^{15}N-labeled, ^{13}C-His enriched *A. variabilis* plastocyanin

Uniformly ^{15}N, ^{13}C-His enriched *A. variabilis* plastocyanin was heterologously produced in *Escherichia coli* BL21(DE3) from the previously described strain (Hass

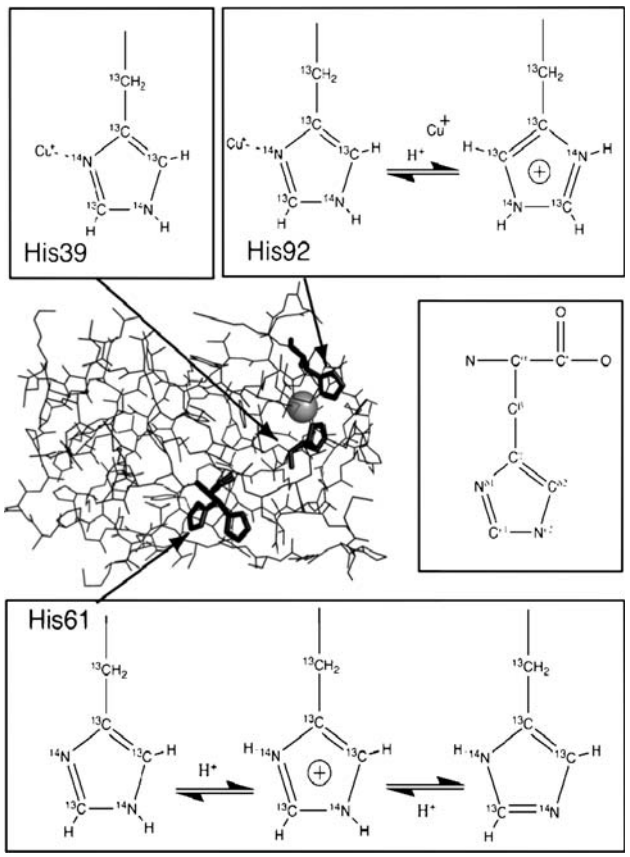

Fig. 1 *Upper and middle panel*: the three histidine residues in *A.v.* PCu and their protonation states and locations in the crystal structure (Schmidt et al. 2006). The two copper coordinating histidines are His39 and His92, where only His92 protonates. *Lower panel*: the two different orientations of the His61 imidazole side chain that are stabilized by hydrogen bonding; in one orientation the δ-tautomer is stabilized in the other the ε-tautomer. The isotope labels indicated in the figure correspond to the labeling used in this work

et al. 2008a) by fed-batch cultivation (Schmidt et al. 2006) with the following modifications. After depletion of the glucose, portions of 0.8 g glucose (from 4 g/l stock solution) were added until the initial NH_4Cl was depleted. Subsequently 0.6 g $^{15}NH_4Cl$ (>99% ^{15}N enriched, Spectra Stable Isotope) and 25 mg ^{13}C-histidine, HCl (98% ^{13}C enriched, Cambridge Isotope Laboratories, CLM-2264, U-13C6) were added. After the next oxygen spike 3.9 g $^{15}NH_4Cl$ and 100 mg ^{13}C-histidine, HCl were added and the plastocyanin expression induced by addition of IPTG as previously described (Schmidt et al. 2006; Hass et al. 2008a). After 2 h, cells were harvested and the plastocyanin purified as previously described (Schmidt et al. 2006). Approximately 50 mg per liter of culture of pure plastocyanin with a peak ratio of A_{278}/A_{597} of 1.12 was obtained. Finally, the purified oxidized plastocyanin was reduced with a fivefold molar excess of sodium ascorbate for 1 h at +4°C. Excess ascorbate was removed and the protein exchanged into a 5% D_2O/95% H_2O 50 mM NaCl solution and concentrated to 1.0 mM by ultrafiltration using a stirred ultrafiltration cell (Amicon) fitted with a 3 kDa cutoff membrane.

NMR samples

All samples contained 1.0 mM ^{13}C-His labeled reduced A.v. PCu in 5% D_2O/95% H_2O with 50 mM NaCl. Small amounts of sodium ascorbate were added in order to keep the protein reduced. The sample used for the chemical shift titration contained 20 mM sodium acetate buffer and 20 mM sodium phosphate buffer. NMR samples used for CPMG dispersion contained no buffer.

NMR spectroscopy

All NMR experiments were carried out at a field strength of 11.7 T corresponding to resonance frequencies of 500 MHz and 125.7 MHz of ^1H and ^{13}C nuclei, respectively, using a Varian Inova spectrometer equipped with a cold probe. The pH dependence of the ^{13}C chemical shifts of the histidine imidazole side-chain was determined from a series of constant time (CT) ^{13}C HSQC spectra recorded at 12 different pH values in the range from pH = 4.0 to pH 8.5. The CT version of the ^{13}C HSQC experiment was chosen to eliminate the effect from the scalar ^{13}C coupling between the $^{13}C^{\delta 2}$ and $^{13}C^{\gamma}$ (Vuister and Bax 1992). The CT delay was set to 16 ms. The sweep widths were set to 5.0 kHz in both the ^{13}C and ^1H dimension. The number of complex data points acquired in the two dimensions was 160 and 512, respectively.

The pH dependences of the chemical shifts were analyzed according to a single titration unaffected by other titrations in the protein:

$$\delta = \delta_0 + \frac{\Delta\delta}{1 + 10^{[\mathrm{pH}-\mathrm{p}K_a]}} \quad (1)$$

where δ_0 is the chemical shift of the deprotonated form and $\delta_0 + \Delta\delta$ is the chemical shift of the protonated form.

The pulse sequences used to monitor the ^{13}C CPMG dispersion were those used for conventional ^{15}N CT-CPMG dispersion experiments (Tollinger et al. 2001). The ^{13}C and ^{15}N channels were interchanged using the "rfchannel" command in VnmrJ software (Varian Inc.). The length of each INEPT (insensitive nuclei enhanced by polarization transfer) and refocusing periods outside the CPMG delay were 2.5 ms assuming a scalar coupling constant $J_{^{13}C-^1H}$ of $\sim$200 s^{-1}. The sweep widths were set to 1.76 kHz and 5.0 kHz in the ^{13}C and ^1H dimension, respectively. The ^{13}C sweep width was chosen so that overlap between the $^{13}C^{\varepsilon 1}$-signals and the folded $^{13}C^{\delta 2}$-signals was avoided and the ^{13}C carrier frequency was set at 138.5 ppm. A series of 16 and 512 complex data were recorded in the ^{13}C and ^1H dimension, respectively. The

total CPMG relaxation time, Δ, was 20 ms. A series of 16 2D-planes were recorded with different CPMG fields, ν_{CPMG}, ranging from 50 to 1,900 Hz. An additional plane with a CPMG relaxation time of 0 ms was also recorded. The CPMG field strength is defined as $\nu_{CPMG} = 1/(2\tau_{cp})$, where τ_{cp} is the delay between the 180° pulses in the CPMG period. The B_1 field strength of the 180° ^{13}C CPMG pulses was 9.6 kHz. GARP ^{13}C-decoupling was used during acquisition. Temperature was calibrated against a methanol sample. Effective R_2 rates, R_2^{eff}, were calculated from the signal intensities, $I(\nu_{CPMG})$ and I_0, using $R_2^{eff} = \Delta^{-1}\ln(I_0/I(\nu_{CPMG}))$ where I_0 is the intensity in the 2D-plane without the CPMG delay. Errors were estimated as the average standard deviation of double measurements made at three different CPMG field strengths.

The CPMG dispersion data were analyzed using a two-site exchange model and assuming fast exchange ($k_{ex} > \Delta\omega$) (Luz and Meiboom 1963)

$$R_2^{eff} = R_2^0 + \Delta\omega^2 p_A p_B \frac{1}{k_{ex}}\left[1 - \frac{4\nu_{CPMG}}{k_{ex}}\tanh\left(\frac{k_{ex}}{4\nu_{CPMG}}\right)\right] \quad (2)$$

where R_2^0 is the effective R_2 rate at infinitely strong CPMG fields, $\Delta\omega = \gamma B_0 \Delta\delta$ is the difference in frequency between the two conformations, γ is the gyromagnetic ratio, $\Delta\delta$ the difference in chemical shift of a given nucleus in the two exchanging forms, p_A and p_B are the populations of the two forms, and k_{ex} is the exchange rate.

Results and discussion

Chemical sift titration

Chemical shift information is valuable in CPMG studies of exchange processes. In the case of exchange, titration data provide information about the chemical shift difference, $\Delta\delta$, of a nucleus in various exchanging states. If these processes are in the slow ($k_{ex} < \Delta\omega$) or intermediate ($k_{ex} \approx \Delta\omega$) exchange regime the obtained $\Delta\delta$ values provide an independent check of the $\Delta\delta$ values derived from the CPMG dispersion curves together with the exchange rate, k_{ex}, and the populations p_A and p_B, (see Eq. 2). In the case of fast exchanging processes, such as the exchange between the histidine protonation states studied here (see above) they are indispensible in order to extract k_{ex} from the dispersion curves.

Here, a series of CT-HSQC spectra were recorded at different pH in order to monitor the titration of the ^{13}C chemical shifts. Buffer was added to ensure pH stability and fast protonation equilibria (Hass et al. 2007). At pH 6.5 all six signals from the three histidines are observed (see Fig. 2). At higher pH the $^{13}C^{\delta 2}$-signal of His61 decreases in intensity and disappears above pH 8 (Fig. 2B) while the $^{13}C^{\varepsilon 1}$-signal moves substantially and broadens slightly at alkaline pH (Fig. 2A). (Note that resonance broadening in the ^{13}C dimension of the CT-HSQC spectrum will only appear as an intensity loss. The ^{13}C linewidth is defined

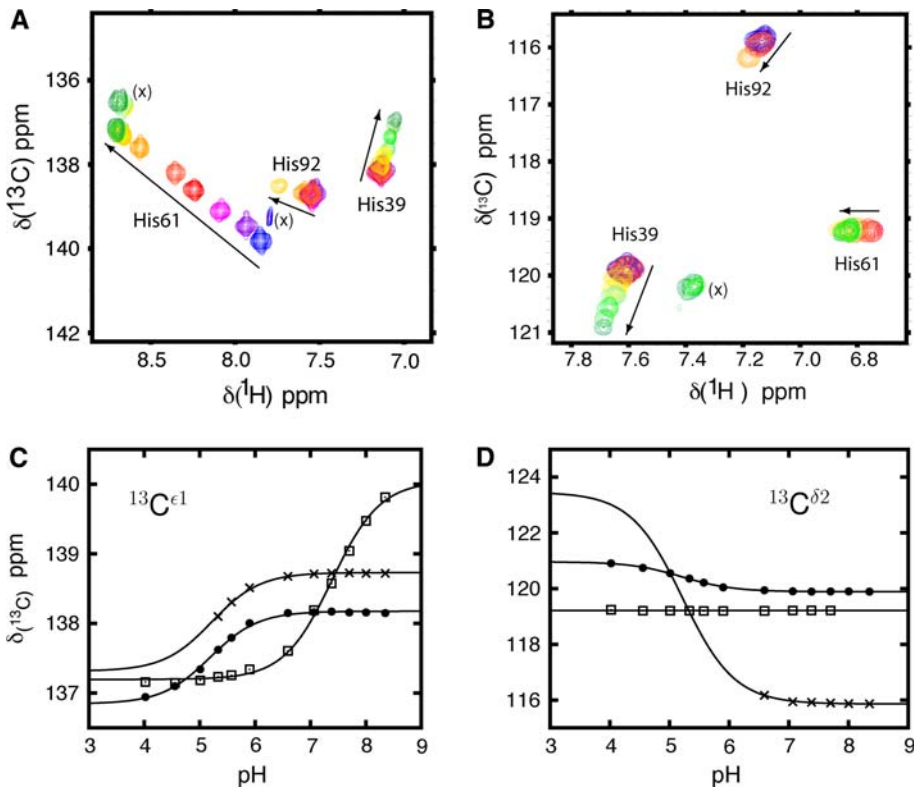

Fig. 2 *Upper panel*: Overlay of ^{13}C CT-HSQC spectral regions showing the imidazole CH groups in *A.v.* PCu at 3.5°C and 12 different pH values ranging from pH 8.5 (*blue*) through pH 7.4 (*red*) and pH 5.5 (*yellow*) to pH 4.0 (*green*). **A** Region showing the $^{13}C^{\varepsilon 1}$ signals; **B** Region showing the $^{13}C^{\delta 2}$ signals. The *arrows* indicate the direction in which the peaks move with increasing H^+ concentration; (*x*) denotes peaks from impurities, most likely from denatured protein formed at extreme pH values. *Lower panel*: Chemical shift titration curves of **C** The $^{13}C^{\varepsilon 1}$ carbons and **D** $^{13}C^{\delta 2}$ carbons, of His39 (●), His61 (⊡), and His92 (✖). The chemical shift data versus pH were analyzed using Eq. 1. The fitted parameters are given in Table 1

Table 1 Parameters[a] derived from ^{13}C and ^{1}H chemical shift titration data obtained from ^{13}C HSQC spectra[b] of the three histidine residues in *A.v.* plastocyanin at 3.5°C

Residue	Nucleus	$\Delta\delta$ (ppm)	pK_a	δ_0 (ppm)
H39	$^{13}C^{\varepsilon1}$	−1.33(0.03)	5.19(0.03)	138.18(0.01)
H39	$^{13}C^{\delta2}$	1.07(0.01)	5.21(0.02)	119.89(0.01)
H61	$^{13}C^{\varepsilon1}$	−2.85(0.06)	7.39(0.03)	140.05(0.06)
H61	$^{13}C^{\delta2}$	0.00(0.01)	–	119.21(0.01)
H92	$^{13}C^{\varepsilon1}$	−1.41(0.03)	5.22[c]	138.73(0.01)
H92	$^{13}C^{\delta2}$	7.52(0.43)	5.22[c]	115.86(0.01)
H39	$^{1}H^{\varepsilon1}$	−0.10(0.01)	5.15(0.06)	7.135(0.001)
H39	$^{1}H^{\delta2}$	0.09(0.01)	5.38(0.04)	7.605(0.001)
H61	$^{1}H^{\varepsilon1}$	0.91(0.02)	7.37(0.03)	7.776(0.016)
H61	$^{1}H^{\delta2}$	0.13(0.01)	7.15(0.09)	6.694(0.009)
H92	$^{1}H^{\varepsilon1}$	1.27(0.02)	5.22[c]	7.536(0.005)
H92	$^{1}H^{\delta2}$	1.16(0.11)	5.22[c]	7.128(0.002)

[a] Equation 1; standard deviations are given in brackets

[b] Recorded at 12 pH values in the range from pH = 4.0 to pH = 8.5

[c] pK_a was fixed at this value during the fitting of Eq. 1

solely by the window functions and remains unchanged throughout the titration series). The pK_a value of 7.4 obtained from fitting (Eq. 1) to the titration data agrees with previous values of the pK_a of His61 (see Table 1). Clearly the $^{13}C^{\varepsilon1}$ is in fast exchange between protonated and deprotonated forms of His61 because the titration curve is continous (Fig. 2C). The $^{13}C^{\delta2}$–$^{1}H^{\delta2}$ cross-peak, which is highly sensitive to tautomerization disappears at pH > 8 most likely because of slow ($k_{ex} < \Delta\omega$) or intermediate ($k_{ex} \approx \Delta\omega$) tautomer exchange that occurs when the imidazole ring of His61 is deprotonated and the buffer system is shifted towards alkaline values (Hass et al. 2008a). The disappearance of this cross-peak at pH > pK_a suggests that His61 not only undergoes protonation, but also undergoes conformational exchange when deprotonated, most likely tautomerization, in agreement with previous findings (Hass et al. 2008a). Curiously, the $^{13}C^{\delta2}$ resonance of His61 (opposite the $^{13}C^{\varepsilon1}$ resonance) does not move upon protonation of His61. In contrast, the corresponding signals of His39 and His92 are all affected by the protonation of His92. At acidic pH the $^{13}C^{\varepsilon1}$–$^{1}H^{\varepsilon1}$ and $^{13}C^{\delta2}$–$^{1}H^{\delta2}$ cross-peaks from His92 disappear because of exchange broadening in the ^{1}H dimension (Fig. 2).

CPMG dispersion

The CPMG dispersion techniques can detect exchange processes with exchange rate, k_{ex}, that are within the range of 100–10,000 s^{-1}, depending on the chemical shift difference, $\Delta\omega$ between the exchanging site, the population, p_A and p_B of these sites, and the CPMG field strength $\nu_{CPMG} = 1/(2\tau_{cp})$, (Eq. 2). The most critical experimental conditions that influence the exchange rate, and/or the populations p_A and p_B are the pH, the temperature, and the buffer concentration, all of which can be adjusted to make the exchange process detectable by CPMG dispersion experiments. In particular, protonation rates are likely to be general acid/base catalyzed where the exchange rate increases linearly with the buffer concentration (Hass et al. 2007). If this is the case, as it is in *A.v.* PCu, the buffer concentration should be kept as low as possible to ensure that protonation occurs sufficiently slowly. Consistent with our previous ^{15}N CPMG studies (Hass et al. 2004, 2008a), the ^{13}C CPMG studies here confirm that below 10°C and at low buffer concentrations (<1 mM) the proton exchange rates in *A.v.* PCu enter a regime where the exchange between protonation states can be monitored by standard CPMG dispersion experiments ($k_{ex} < 5{,}000\ s^{-1}$).

The ^{13}C chemical shifts and R_2^{eff} rates of His92 and His39 are both strongly affected by the protonation of His92. Even though His39 does not undergo protonation, its change in ^{13}C chemical shift upon titration of His92 is similar to that of His92 and the dispersion profiles for the two residues are similar (Fig. 3B, D). Indeed, the rates obtained from the dispersion curves of His39 ^{13}C nuclei are in excellent agreement with rates obtained previously from the backbone ^{15}N nuclei (Hass et al. 2004, 2008a) as shown in Fig. 4B. The results of the CPMG dispersion experiments can be validated by comparing them with the results of the chemical shift titrations, which provide independent information about the populations and chemical shift differences between protonated and deprotonated forms. The comparison can also establish the nature of the exchange process observed in the CPMG dispersion experiment. Thus, since only the product $p_A p_B|\Delta\delta|^2$ can be obtained from CPMG dispersion data in the case of fast exchange, we fixed the populations to those obtained from the chemical shift titrations and determine $|\Delta\delta|$ or, vice versa, fixed the chemical shift differences to those obtained from ^{13}C chemical shift titration and determine the populations. In both cases mutually consistent values are obtained for His39 and His92 at pH 6.5 as shown in Table 2. This consistency confirms that the dispersions observed for His92 and His39 are caused by the exchange between protonated and deprotonated His92.

For His92 itself, the ^{13}C dispersion profiles are hampered by the decreasing signal intensity as the pH value approaches the pK_a value. This problem also occurs for His61 (pK_a = 7.4) for which the signal disappears between pH 6.5–8 at low buffer concentrations (not shown). At pH 9.5 the His61 signal is clearly visible and shows small but significant dispersion (Fig. 3C). At this pH the dispersion effect here can not be caused by the protonation/deprotonation equilibrium because <1% of His61 is protonated

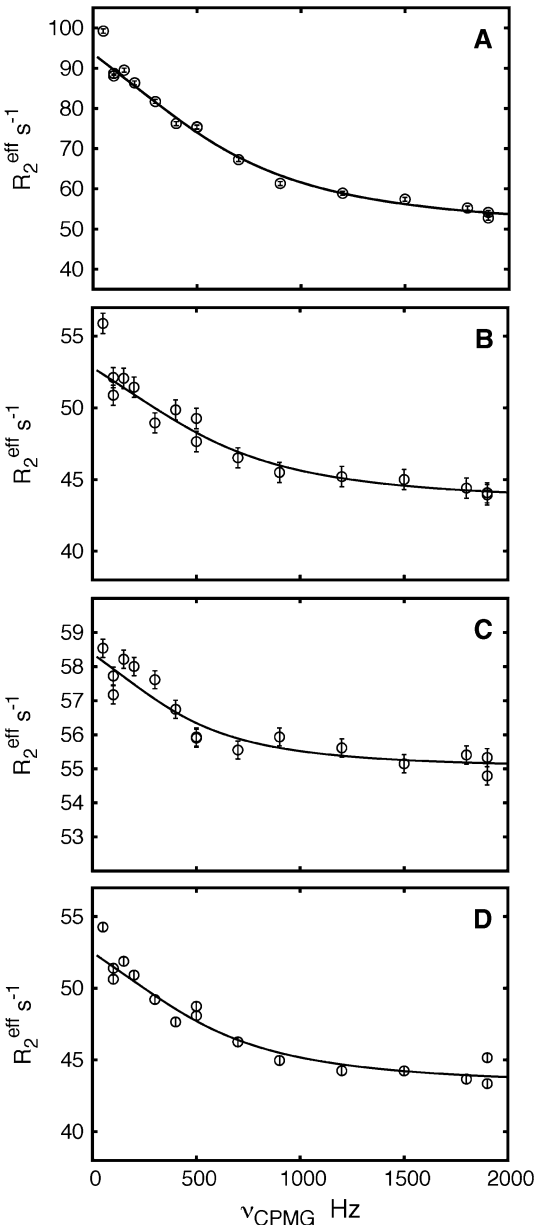

Fig. 3 $^{13}C^{\varepsilon 1}$ CPMG dispersion curves **A** His39 (pH 5.9 and 3.5°C), **B** His39 (pH 6.5 and 8.5°C), **C** His61 (pH 9.5 and 3.5°C), **D** His92 (pH 6.5 and 8.5°C)

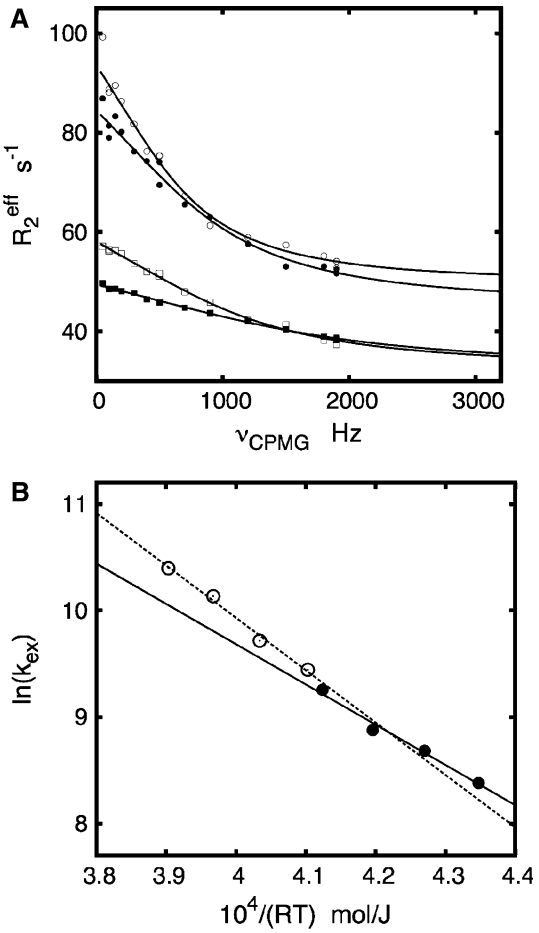

Fig. 4 **A** CPMG dispersion curves of His39 at pH 5.9, without buffer added and at four different temperatures: (⊙) 3.5°C (●) 8.5°C (⊡) 13.5°C (■) 18.5°C; **B** Arrhenius' plot showing the agreement between the exchange rates for the protonation of His92 obtained from ^{13}C CPMG dispersion (●) and the exchange rates calculated from previously obtained backbone ^{15}N relaxation data (⊙) (Hass et al. 2004). The calculation of the latter rates requires the pK_a value of His92, which depends on the temperature. In contrast to previously published values (Hass et al. 2004) the temperature dependence of pK_a is here taken into account (see Table 2, footnote a). The activation energies, E_A, derived from the slopes obtained in **B** for the two data sets (●) and (⊙) are 38 and 49 kJ/mol, respectively, according to the Arrhenius equation, $k_{ex} \propto \exp(-E_A/RT)$

(Hass et al. 2008a). In stead it is caused by the tautomerization of His61, as indicated by the agreement between the exchange rate of $(2.8 \pm 0.7)10^2$ s^{-1} obtained here at pH 9.5 and the exchange rate of $(2.2 \pm 0.2)10^2$ s^{-1} obtained previously for the tautomerization reaction of His61 under similar conditions using backbone ^{15}N and ^{1}H CPMG dispersion (Hass et al. 2008a). Thus, in the case of *A.v.* PCu the ^{13}C dispersion experiments information is obtained about (1) protonation and deprotonation of the imidazole ring of His92, (2) tautomerization of the imidazole ring of His61, and (3) a rearrangement of the side chain of His39 or its environment caused by His92 protonation. These three types of processes and monitoring of them using ^{13}C CPMG dispersion are discussed in the following three sections.

Imidazole protonation

Protonation equilibria of histidine residues are common at physiological condition. These equilibria can cause NMR signals to broaden significantly or even lead to complete loss of signals (Sudmeier et al. 1980; Hass et al. 2004, 2008a), dependent on the pH, exchange rate, k_{ex}, and the difference in

Table 2 Parameters[a] derived from the CPMG dispersion and chemical shift titration data obtained for the three histidine residues in *A.v.* plastocyanin

	$\lvert\Delta\delta\rvert$ (CPMG)[b] ppm	$\lvert\Delta\delta\rvert$ (titration)[c] ppm	$p_A p_B$ (titration)	$p_A p_B$ (CPMG)[d]	k_{ex} (CPMG) s^{-1}	R_2^0 (CPMG) s^{-1}	T°C	pH
His92 protonation/deprotonation								
H39	1.46(0.06)	1.33(0.03)	0.143[f]	0.175(0.015)	4355(312)	49.8(1.2)	3.5	5.9
H39	1.64(0.14)	1.33(0.03)	0.136[f]	0.211(0.034)	5898(743)	45.5(2.2)	8.5	5.9
H39	1.5[e]	1.33(0.03)	0.130[f]	–	7159(97)	32.6(0.2)	13.5	5.9
H39	1.5[e]	1.33(0.03)	0.124[f]	–	10449(103)	32.6(0.1)	18.5	5.9
H39	1.24(0.11)	1.33(0.03)	0.043[f]	0.035(0.006)	4005(650)	43.4(0.5)	8.5	6.55
H92	1.18(0.11)	1.41(0.03)	0.043[f]	0.028(0.005)	3699(635)	43.2(0.5)	8.5	6.55
His61 tautomerization								
H61	0.45(0.06)	–	0.081[g]	–	2833(685)	55.0(0.3)	3.5	9.50

[a] Equations 1 and 2; standard deviations are given in brackets

[b] Calculated using the populations obtained from chemical shift titration, see f and g

[c] All values are determined at 3.5°C

[d] Calculated using $\lvert\Delta\delta\rvert$ obtained from chemical shift titrations

[e] $\Delta\delta$ was fixed at the average of the values determined at the two lowest temperatures. Only k_{ex} and R_2^0 were optimized in the fit

[f] Using $pK_a = 5.22$ (3.5°C, this work) and $pK_a = 5.09$ (25°C, (Hass et al. 2004)). At the other temperatures pK_a was obtained using $-RT \ln K_a = \Delta H° - T\Delta S°$ where $\Delta H°$ and $\Delta S°$ are 9.5 kJ/mol and −65 J/(mol K), respectively

[g] Hass et al. 2008a

chemical shift, $\Delta\delta$. In the case of imidazole exchange processes the ^{13}C CPMG dispersion experiments are useful, because the ^{13}C chemical shifts are affected only moderately by imidazole protonation (the $\Delta\delta$ values being of the order of 1 ppm, corresponding to $\Delta\omega = 786$ rad/s, at 11.7 Tesla) and the ^{13}C signals therefore are unlikely to be affected by severe linebroadening. Thus, in the case of surface exposed histidines where protonation equilibria typically are faster than 1,000 s^{-1} (Eigen 1963; Sudmeier et al. 1980; Hass et al. 2007, 2008a), the exchange process is in fast exchange ($k_{ex} > \Delta\omega$) with respect to ^{13}C nuclei and the observed signals are therefore relatively narrow. This contrasts the imidazole ^{15}N nuclei, which experience much larger shifts (Pelton et al. 1993) (~80 ppm, corresponding to $\Delta\omega = 25{,}000$ rad/s at 11.7 Tesla), and the exchange process is therefore in the slow or intermediate regime for typical imidazole protonation exchange rates. This, in turn, results in excessive line broadening and loss of signals at exchange rates where relaxation dispersion experiments are useful. In proton detected ^{13}C experiments proton signal broadening may be a problem, as observed for the $^{13}C^{\varepsilon 1}$ nucleus of His61 and His92 where the line broadening of the protons is larger than the line broadening of ^{13}C. This leads to a severe loss of signal intensity in the ^{13}C CPMG dispersion experiment and makes it difficult to monitor the protonation of the imidazole group at pH ≈ pK_a where the population of the protonated and deprotonated forms are of the same magnitude. For His92 a sufficiently good signal-to-noise ratio was obtained only for a relatively slow exchange rate in the absence of buffer, and only at pH values relatively far from the pK_a value (pH = 6.5) where the protonated form is only 5% populated (Fig. 3C). The skewed population enhances the signal-to-noise ratio, however, it also reduces the CPMG dispersion (Eq. 2), which therefore becomes difficult to detect. The signal-to-noise ratio can also be improved if, instead, the exchange process is brought into the fast exchange regime by increasing the exchange rate, k_{ex}, and thereby reducing the linebroadening. This can be done by adding buffers or by raising the temperature. However, in addition to a reduced CPMG dispersion, an increased k_{ex} also leads to more linear CPMG dispersion profiles, from which it is difficult to obtain reliable values of k_{ex} and the chemical shift difference $\Delta\delta$. The same problems were observed for His61. Therefore, reliable dispersion curves reporting on the protonation and deprotonation of His61 were not obtained.

Imidazole tautomerization

For free histidine the ε-tautomer is favored over the δ-tautomer by the ratio 4:1 (Reynolds et al. 1973). In proteins this ratio can be very different, however both tautomer forms are commonly found in proteins. The tautomer equilibrium can give rise to exchange phenomena, as in the case of His61 in *A.v.* PCu. Thus, His61 is not only affected by protonation but also undergoes a tautomerization where the ε-tautomer is favored by a ratio 9:1 (Hass et al. 2008a). At pH = 9.5 His61 is only affected by the tautomerization while the effect from protonation is insignificant because the protonated form is only ~1% populated. Therefore, at high pH the dispersion curves of His61 (Fig. 3B) can be analyzed according to the

two-site model (Eq. 2). Yet the dispersion of the $^{13}C^{\varepsilon 1}$ carbon is relatively small ($|\Delta\delta| = 0.4$ ppm) suggesting that at least in the case of His61 the $^{13}C^{\varepsilon 1}$ carbon is only moderately sensitive to tautomerization.

In contrast, previous studies show that $^{13}C^{\delta 2}$ is strongly affected by tautomerization with a chemical shift difference, $\Delta\delta$, between the two tautomeric forms of up till 10 ppm (Sudmeier et al. 2003). In qualitative agreement with this the $^{13}C^{\delta 2}$-signal of His61 disappears with increasing exchange rate at high pH (Fig. 2B). The disappearance of the signal at pH $\gg$ pK_a suggests that the process is in slow or intermediate exchange at 11.7 Tesla. Therefore, since the exchange rate is $\sim$2,800 s^{-1} (Table 2) $\Delta\delta$ must be >3 ppm. The large chemical shift fluctuation cannot be explained by a protonation/deprotonation process because it occurs at pH $\gg$ pK_a where the signal is unaffected by this process (see above). Rather large chemical shift fluctuation suggests a conformational change of the imidazole side chain of His61 in accordance with previous studies (Hass et al. 2008a), which showed that the imidazole ring of His61 tautomerizes (see Fig. 1, lower panel). The $^{13}C^{\delta 2}$ $\Delta\delta$ value of $\sim$10 ppm reported previously for imidazole tautomerization (Sudmeier et al. 2003) agrees well with the $\Delta\delta$ value larger than 3 ppm suggested by this work. Finally, unlike the $^{13}C^{\delta 2}$-signal of His61, the $^{13}C^{\delta 2}$-signals of His39 and His92 show no linebroadening at high pH, which indicates the absence of tautomerization equilibria for these residues at high pH, and shows that the copper binding prevents tautomerization.

Because of the larger titration shift observed for $^{13}C^{\delta 2}$ compared to $^{13}C^{\varepsilon 1}$, $^{13}C^{\delta 2}$ is potentially a useful reporter on tautomerization processes, provided that the $^{13}C^{\delta 2}$-signal can be observed. Unfortunately CPMG dispersion measurements on $^{13}C^{\delta 2}$ are hampered by the large scalar coupling ($\sim$70 Hz) between $^{13}C^{\delta 2}$ and $^{13}C^{\gamma}$, although this problem could be solved using selectively labeled histidine with NMR inactive ^{12}C in the γ-position. Methods for achieving this kind of selective labeling have been developed recently (Teilum et al. 2006).

Other exchange processes

Although His39 neither protonates nor tautomerizes, it is clearly affected by chemical exchange (Fig. 3A). Therefore, the pH dependent changes in ^{13}C chemical shift of His39 must be caused by the titration of other groups in its vicinity, in this case His92. Indeed, the exchange rate obtained from the CPMG dispersion curve of His39 is in good agreement with the exchange rate of His92, while $\Delta\delta$ value of His39 also derived from the dispersion curve is in good agreement with the $\Delta\delta$ value obtained from the titration of His39 (see Table 2). Finally, the temperature dependence of the rate agrees with that obtained previously from ^{15}N relaxation data (Fig. 4B).

The changes in chemical shift observed for His39 may arise from a conformational change of the copper site, which results from the protonation of His92 (Guss et al. 1986), or they may be caused by the enhanced positive charge of the metal site of PCu (Hass et al. 2008b). However, irrespective of the origin it is interesting that His39 provides the best CPMG dispersion curves for monitoring the His92 protonation. Most likely, this is because His92 protonation causes less line broadening in the proton dimension of the His39 signal than of the His92 signal, which gives a significantly better signal-to-noise ratio for His39 than for His92.

Conclusions

The imidazole $^{13}C^{\varepsilon 1}$ and $^{13}C^{\delta 2}$ titration curves provide information about the protonation states of the imidazole ring and confirm the pK_a values of His92 and His61 in *A.v.* PCu found previously (Hass et al. 2004), while the $^{13}C^{\varepsilon 1}$ CPMG dispersion curves provide quantitative information on the rate of protonation and the associated chemical shift changes. The obtained rate constants are in good agreement with those obtained previously from backbone ^{15}N relaxation studies, yet the ^{13}C approach used here is experimentally simpler and more direct than the usual approach that relies on backbone ^{15}N measurements.

In studies of active sites containing functionally active histidines and in studies of metal sites with histidine ligands, information on the conformation and dynamics of histidine side chains is of particular interest. The ^{13}C CPMG dispersion experiments on the imidazole $^{13}C^{\varepsilon 1}$ provide a straightforward method for studying the dynamics within these sites, dynamics that may be directly coupled to the function of the protein. If selective ^{13}C histidine labeling is used, as in the present study, the approach can be applied even to relatively large proteins. TROSY based CPMG dispersion experiments are available (Loria et al. 1999b) and could further improve the applicability to larger proteins, as deuteration of non-exchangeable non-histidine proton sites could improve the sensitivity of the TROSY experiments. Our study here, as well as previous studies (Kovrigin and Loria 2006) show that imidazole ^{13}C CPMG dispersion is a useful and straightforward tool to obtain detailed insight onto the dynamics associated with histidines and can complement or substitute the more established NMR techniques to study histidine dynamics, i.e. CPMG dispersion experiments on backbone ^{15}N and ^{1}H (Hass et al. 2004, 2008a; Kovrigin and Loria 2006; Grey et al. 2006), and imidazole ^{1}H and ^{15}N line shape analyses (Sudmeier et al. 1980; Hass et al. 2008a). Together with these techniques the ^{13}C experiments presented here form a broad suite of experiments that is highly useful for studying functional dynamics

of histidine containing active sites in enzymes and other proteins.

Acknowledgments We thank Lise-Lotte Jespersen for technical assistance. This study was supported by the Danish Agency for Science, Technology and Innovation, grants, 21-04-0519 and 272-07-0466, Carlsbergfondet grant 1624/40, Novo Nordisk Fonden grant 2003-11-28, and Villum Kann Rasmussen Fonden grant 8.12.2003.

References

Badsberg U, Jørgensen AMM, Gesmar H, Led JJ, Hammerstad JM, Jespersen LL, Ulstrup J (1996) Solution structure of reduced plastocyanin from the blue-green alga *Anabaena variabilis*. Biochemistry 35:7021–7031

Day RM, Thalhauser CJ, Sudmeier JL, Vincent MP, Torchilin EV, Sanford DG, Bachovchin CW, Bachovchin WW (2003) Tautomerism, acid-base equilibria, and H-bonding of the six histidines in subtilisin BPN by NMR. Protein Sci 12:794–810

Eigen M (1963) Protonenübertragung, Saure-Base-Katalyse und enzymatische hydrolyse. 1. Elementarvorgange. Angew Chem 75:489–508

Fersht A (1998) Structure and mechanism in protein science: a guide to enzyme catalysis and protein folding. W. H. Freeman and Company, New York

Grey MJ, Tang YF, Alexov E, McKnight CJ, Raleigh DP, Palmer AG (2006) Characterizing a partially folded intermediate of the villin headpiece domain under non-denaruring conditions: contribution of His41 to the pH-dependent stability of the N-terminal subdomain. J Mol Biol 355:1078–1094

Guss JM, Harrowell PR, Murata M, Norris VA, Freeman HC (1986) Crystal-structure analyses of reduced (CuI) poplar plastocyanin at 6 pH values. J Mol Biol 192:361–387

Hass MAS, Thuesen MH, Christensen HEM, Led JJ (2004) Characterization of μs-ms dynamics of proteins using a combined analysis of N-15 NMR relaxation and chemical shift: conformational exchange in plastocyanin induced by histidine protonations. J Am Chem Soc 126:753–765

Hass MAS, Christensen HEM, Zhang JD, Led JJ (2007) Kinetics and mechanism of the acid transition of the active site in plastocyanin. Biochemistry 46:14619–14628

Hass MAS, Hansen DF, Christensen HEM, Led JJ, Kay LE (2008a) Characterization of conformational exchange of a histidine side chain: protonation, rotamerization, and tautomerization of his61 in plastocyanin from *Anabaena Variabilis*. J Am Chem Soc 130:8460–8470

Hass MAS, Jensen MR, Led JJ (2008b) Probing electric fields in proteins in solution by NMR spectroscopy. Proteins 72:333–343

Ishima R, Torchia DA (2003) Extending the range of amide proton relaxation dispersion experiments in proteins using a constant-time relaxation-compensated CPMG approach. J Biomol NMR 25:243–248

Kovrigin EL, Loria JP (2006) Enzyme dynamics along the reaction coordinate: critical role of a conserved residue. Biochemistry 45:2636–2647

Loria JP, Rance M, Palmer AG (1999a) A relaxation-compensated Carr-Purcell-Meiboom-Gill sequence for characterizing chemical exchange by NMR spectroscopy. J Am Chem Soc 121:2331–2332

Loria JP, Rance M, Palmer AG (1999b) A TROSY CPMG sequence for characterizing chemical exchange in large proteins. J Biomol NMR 15:151–155

Luz Z, Meiboom S (1963) Nuclear magnetic resonance study of protolysis of trimethylammonium ion in aqueous solution - order of reaction with respect to solvent. J Chem Phys 39:366–370

Mandel M (1965) Proton magnetic resonance spectra of some proteins. I. Ribonuclease oxidized ribonuclease lysozyme and cytochrome c. J Biol Chem 240:1586–1592

Markley JL (1975) Observation of histidine residues in proteins by means of nuclear magnetic-resonance spectroscopy. Accounts Chem Res 8:70–80

Palmer AG, Kroenke CD, Loria JP (2001) Nuclear magnetic resonance methods for quantifying microsecond-to-millisecond motions in biological macromolecules. Method Enzymol 339:204–238

Pelton JG, Torchia DA, Meadow ND, Roseman S (1993) Tautomeric states of the active-site histidines of phosphorylated and unphosphorylated III(Glc), a signal-transducing protein from *Escherichia coli*, using two-dimensional heteronuclear NMR techniques. Protein Sci 2:543–558

Perez-Canadilllas JM, Garcia-Mayoral MF, Laurents DV, del Pozo AM, Gavilanes JG, Rico M, Bruix M (2003) Tautomeric state of a-sarcin histidines. Nδ tautomers are a common feature in the active site of extracellular microbial ribonucleases. FEBS Lett 534:197–201

Reynolds WF, Peat IR, Freedman MH, Lyerla JR (1973) Determination of tautomeric form of imidazole ring of l-histidine in basic solution by C-13 magnetic-resonance spectroscopy. J Am Chem Soc 95:328–331

Schmidt L, Christensen HEM, Harris P (2006) Structure of plastocyanin from the cyanobacterium *Anabaena variabilis*. Acta Crystallogr D 62:1022–1029

Shimahara H, Yoshida T, Shibata Y, Shimizu M, Kyogoku Y, Sakiyama F, Nakazawa T, Tate S, Ohki S, Kato T, Moriyama H, Kishida K, Tano Y, Ohkubo T, Kobayashi Y, Ha (2007) Tautomerism of histidine 64 associated with proton transfer in catalysis of carbonic anhydrase. J Biol Chem 282:9646–9656

Sudmeier JL, Evelhoch JL, Jonsson NBH (1980) Dependence of NMR lineshape analysis upon chemical rates and mechanisms - implications for enzyme histidine titrations. J Magn Reson 40:377–390

Sudmeier JL, Bradshaw EM, Haddad KEC, Day RM, Thalhauser CJ, Bullock PA, Bachovchin WW (2003) Identification of histidine tautomers in proteins by 2D H-1/C-13(δ2) one-bond correlated NMR. J Am Chem Soc 125:8430–8431

Teilum K, Brath U, Lundstrom P, Akke M (2006) Biosynthetic C-13 labeling of aromatic side chains in proteins for NMR relaxation measurements. J Am Chem Soc 128:2506–2507

Tollinger M, Skrynnikov NR, Mulder FAA, Forman-Kay JD, Kay LE (2001) Slow dynamics in folded and unfolded states of an SH3 domain. J Am Chem Soc 123:11341–11352

Vuister GW, Bax A (1992) Resolution enhancement and spectral editing of uniformly C-13-enriched proteins by homonuclear broad-band C-13 decoupling. J Magn Reson 98:428–435